ELSEVIER

Contents lists available at ScienceDirect

## Journal of Solid State Chemistry

journal homepage: www.elsevier.com/locate/jssc



# Structural investigations of the Bi<sub>2-x</sub>Sb<sub>x</sub>Te<sub>3-y</sub>Se<sub>y</sub> topological insulator

Husain F. Alnaser<sup>a</sup>, Stacey J. Smith<sup>b</sup>, Taylor D. Sparks<sup>a,c,\*</sup>

- <sup>a</sup> Department of Materials Science and Engineering, University of Utah, Salt Lake City, UT, 84112, USA
- <sup>b</sup> Department of Chemistry & Biochemistry, Brigham Young University, Provo, UT, 84602, USA
- <sup>c</sup> Department of Chemistry, University of Liverpool, Liverpool, L7 3NY, United Kingdom



Keywords: BSTS Single crystal Crystallography Twinning

#### ABSTRACT

Exotic phases of matter such as topological insulators are a captivating class of advanced functional materials. Key to understanding the behavior of topological insulators is elucidating their structure, but this can be challenging. For example,  $Bi_{2-x}Sb_xTe_{3-y}Se_y$  crystals have been extensively grown and studied, yet there is still ambiguity in the literature concerning the crystal structure due to the availability of multiple competing candidate structures and inconsistent use of crystallographic terminology, specifically with respect to structures in the trigonal and hexagonal crystal systems. In this work, we investigate the  $Bi_{2-x}Sb_xTe_{3-y}Se_y$  structure using a variety of techniques including single-crystal and powder X-ray diffraction, electron microscopy, X-ray photoelectron spectroscopy, and X-ray fluorescence. Structure refinement of diffraction data suggests that  $Bi_{2-x}Sb_xTe_{3-y}Se_y$  belongs to the trigonal crystal system having  $R\overline{3}m$  symmetry. X-ray photoelectron spectroscopy analysis supports the refined atomic site occupancies. We present two reasons for the misattribution of  $Bi_{2-x}Sb_xTe_{3-y}Se_y$  to hexagonal symmetry in former literature. First, improper use or misinterpretation of crystallographic terminology has led to crystal symmetry being incorrectly confused with lattice system, crystal family, or unit cell choice. Second, the presence of defects can produce easily misinterpreted diffraction patterns, and we propose that twinning is the primary source of confusion between trigonal and hexagonal symmetry for BSTS.

#### 1. Introduction

Single crystals have played a major role in the development of different applications such as lasers, electronic devices, and semiconductors [1]. This is in part because single crystals tend to have excellent corrosion resistance and electron mobility in addition to conveying control over crystal orientation [2]. The desire to produce single crystals and capitalize on their advantages has inspired numerous innovations in the semiconductor industry, including recent advances in producing organic semiconducting single crystals [3,4]. Such advancements over time have led to better computers in physical size, memory size, operations speed, and overall performance [5]. However, as electronic devices become nanoscaled, a tunneling effect emerges that requires alternate approaches [6]. This has led to the development of quantum materials such as topological insulating materials (TIs) [7,8], which are enabling a new generation of computers (quantum computers) [9].

TIs have attracted the interest of researchers worldwide because of their exotic properties [10-12]. There are a growing number of TIs that have been synthesized and studied. For example,  $TaAs_2$  has a

two-dimensional (2D) topology somewhat like graphene while  $Bi_{1-x}Sb_x$  has a three-dimensional (3D) topology [13]. 3D TIs tend to exhibit excellent electronic transport properties and tunability [14] making them ideal candidates for quantum computing components. However, it has been challenging to make 3D TIs with high-quality crystals and high-performance efficiency until recently. Within the last decade,  $Bi_{2-x}Sb_xTe_{3-y}Se_y$  (BSTS) was identified and has yielded promising results [15,16]. Ever since, BSTS has been among the most studied TIs synthesized and analyzed primarily because it shows excellent electron transport measurements while being relatively easy to synthesize and convert to devices compared with other TIs [17]. For example, Han et al. did a comparative study of BSTS growth methods including melting, Bridgman, and a combined approach that led to high quality crystals [18].

Unfortunately, there are a number of seemingly contradictory reports for the structure of BSTS. Consider, for example, this statement by Ko et al. which states "... the crystal structure of BSTS: a hexagonal crystal structure with a rhombohedral unit cell ..." [19] Consider another example from Lohani et al. "... shows the primitive unit cell of BiSbTeSe2 which has a rhombohedral symmetry. This structure can also be depicted as a hexagonal unit cell as shown ..." [20] Ren et al. stated "All

<sup>\*</sup> Corresponding author. Department of Materials Science and Engineering, University of Utah, Salt Lake City, UT, 84112, USA. *E-mail address:* sparks@eng.utah.edu (T.D. Sparks).

diffraction peaks can be indexed based on the rhombohedral structure with the  $R\overline{3}m$  space group" [21] and Han et al. in our previous work stated it was a "... rhombohedral structure in the  $R\overline{3}m$  space group." [18] Among these four examples, we see that BSTS is reported to have either a rhombohedral or hexagonal crystal structure with either a hexagonal or rhombohedral unit cell.

The confusion in nomenclature extends beyond just scientific literature and can also be seen in scientific software such as CALPHAD (Computer Coupling of Phase Diagrams and Thermochemistry) provided by ThermoCalc. When this software is used to generate a pseudo-binary phase diagram in the Bi-Sb-Te-Se system, the generated phase diagrams suggest the possibility of two different phases corresponding to the BSTS stoichiometry, "hexagonal\_A8" and "rhombohedral\_A7" [22]. These names do not correspond to International Union of Crystallagrophy (IUCr) nomenclature for space group number and symmetry, but likely instead refer to Strukturbericht designation which is an older nomenclature originally developed by Zeitschrift für Kristallographie [23]. In modern IUCr nomenclature, the A7 Strukturbericht designation corresponds to space group 166 with  $R\overline{3}m$  symmetry and A8 Strukturbericht corresponds to space group 152 with  $P3_121$  symmetry [24], and both of these space groups are within the trigonal crystal system.

It is worth noting that CALPHAD predicts that the  $P3_121$  phase is about 3 times more stable than the  $R\overline{3}m$  phase with Gibbs free energies of formation of  $G_{P3_121,f,300C}=-600~kJ/mol$  and  $G_{R\overline{3}mf,300C}=-150~kJ/mol$ , respectively. This thermodyanamic prediction of the  $P3_121$  phase being stable over the  $R\overline{3}m$  phase runs contrary to experimental observations by Ren et al. [21] and Han et al. [18] who both observed the  $R\overline{3}m$  phase.

In this work, we set out to unambiguously determine the structure of BSTS single crystals grown via the Bridgman method using single crystal X-ray diffraction followed by powder diffraction and site-specific compositional analysis via X-ray photoelectron spectroscopy. Based on our findings, we present two reasons for the confusion on  ${\rm Bi}_{2-x}{\rm Sb}_x{\rm Te}_{3-y}{\rm Se}_y$  symmetry in former literature. First, improper use or interpretation of crystallographic terminology has led crystal symmetry to be incorrectly confused with lattice system, crystal family, or unit cell choice. Second, in light of observed X-ray and electron diffraction patterns, we suggest twinning as the primary source of confusion between trigonal and hexagonal symmetry.

## 2. Methods

## 2.1. Materials and synthesis

Elemental Bi, Sb, Te, and Se were ordered from Sigma-Aldrich Co. with a purity of 5 N grade. The raw materials were mixed in a glovebox with a ratio of 1:1:1:2 Bi: Sb: Te: Se. Using a mortar and pestle, the materials were crushed and ground together for 30 min, producing a fine powder with a total weight of 3 g. To facilitate crystal growth, the powder was then sealed in a low pressure, oxygen-free environment inside a carbon-coated quartz tube. The quartz tube was obtained from Technical Glass Products Inc. and had an outer diameter of 14 mm, an inner diameter of 12 mm, and a wall thickness of 2 mm. Prior to loading the powder, we coated the tube with carbon by burning acetone inside it. Excess carbon was gently wiped clean. Once the fine BSTS powder was loaded into the carbon-coated quartz tube, the tube was hooked to an ampoule sealing station where it was subjected to a vacuum pressure of 10<sup>-6</sup> torr and four-flushing cycles with argon gas in order to prevent any oxidation reaction during crystal growth. The final ampoule was 6-8 cm in length. BSTS crystals were then grown using a melt growth method by ramping at 22.9 °C/hr to 550 °C and then holding for two weeks before cooling at a rate of 11.4 °C/min to room temperature.

#### 2.2. Sample characterization

Single crystal XRD. Several BSTS crystals were harvested under oil in ambient conditions and screened before an extremely thin plate (8  $\mu m$   $\times$  $130 \ \mu m \ x \ 271 \ \mu m)$  was found that appeared to be a single crystal. The width and breadth of the crystal were much longer than ideal, but we did not attempt the cut the plate as cutting tended to shatter or crack the crystals. The plate was placed at the tip of a polyimide loop. Lowtemperature (100 K) X-ray diffraction data comprising  $\varphi$ - and  $\omega$ -scans were collected using a Bruker D8 Venture with a kappa goniometer, dual Cu and Mo diamond microfocus X-ray sources, a Bruker Photon-III detector, and an Oxford 800+ low-temperature device. Mo  $K_{\alpha}$  radiation  $(\lambda = 0.71073 \text{ Å})$  was used for this experiment. The Bruker APEX3 suite was used to process the data; reflection intensities were integrated using SAINT, and SADABS was used to apply an absorption correction and scale the data [25]. A numerical absorption correction for strong absorbers was used with a relatively large  $\mu$  \*r value (2.10) derived from the absorption coefficient calculated for the solved structure (57.58) with 0.041 as the equivalent radius. The structure was solved using SHELXT and refined against  $F^2$  on all data by full-matrix least-squares with SHELXL-2014 using established refinement strategies [26-28]. The structure was deposited in the ICSD under CSD 2110541.

Powder XRD. BSTS powder was loaded into a standard cylindrical sample holder (27 mm diameter x 2 mm depth). Room-temperature powder X-ray diffraction data were collected between 8 and  $120^\circ$  2θ with a step size of  $0.008^\circ$ /step in reflection geometry using a PANalytical X'Pert Pro MPD with a Cu sealed tube X-ray source, a Ge monochromator selecting the Cu  $K\alpha_1$  wavelength ( $\lambda=1.540598$  Å), and an X'Celerator detector. Rietveld refinement was performed in Highscore Plus using the single-crystal structure determined previously (CSD 2110541) as the starting structure. Parameters varied during the fit include the scale factor, polynomial background parameters (9), zero shift, specimen displacement, unit cell parameters, z positions for the Bi/Sb and Te1/Se1 atom pairs, Biso for all pairs of atoms, relative occupancies for all pairs of atoms, spherical harmonic parameters (12) to model preferred orientation, and asymmetric profile variables (U, V, W, S/L, D/L, with two peak shape parameters).

Transmission Electron Microscopy. Images of our BSTS material were acquired using a transmission electron microscope (JEOL 2800). The sample was prepared using a focused ion beam (FIB) (FEI HELIOS NANOLAB 650 DUAL BEAM FIB and SEM). The crystal prepared by FIB was coated with Pt and then cut by a laser, producing a nano-size layer of material with a thickness of about 80 nm. TEM-EDS confirmed that the measured area still showed the proper element mix and was representative of the whole sample.

*X-ray Photoelectron Spectroscopy.* The composition of the sample surface was analyzed using X-ray photoelectron spectrometry (XPS) with a KRATOS AXIS ULTRA DLD instrument, NanoFab, surface analysis and imaging lab, University of Utah. The sample was characterized before and after sputtering for 60 s by Ar<sup>+</sup> ion gun.

*X-ray fluorescence.* The composition of the bulk was analyzed using X-ray fluorescence (XRF) with an Eagle III Microspot instrument. The sample was gently cleaved producing a large BSTS layer cross section that was tested under ambient conditions. The sample was cleaved and tested immediately to avoid oxide formation.

## 3. Results and discussion

## 3.1. Single-crystal XRD

Our initial approach for understanding the crystal structure of BSTS was single-crystal X-ray diffraction (XRD). The structure refined well ( $R_1$  = 1.8%, w $R_2$  = 4.3%) in the trigonal crystal system in the rhombohedral

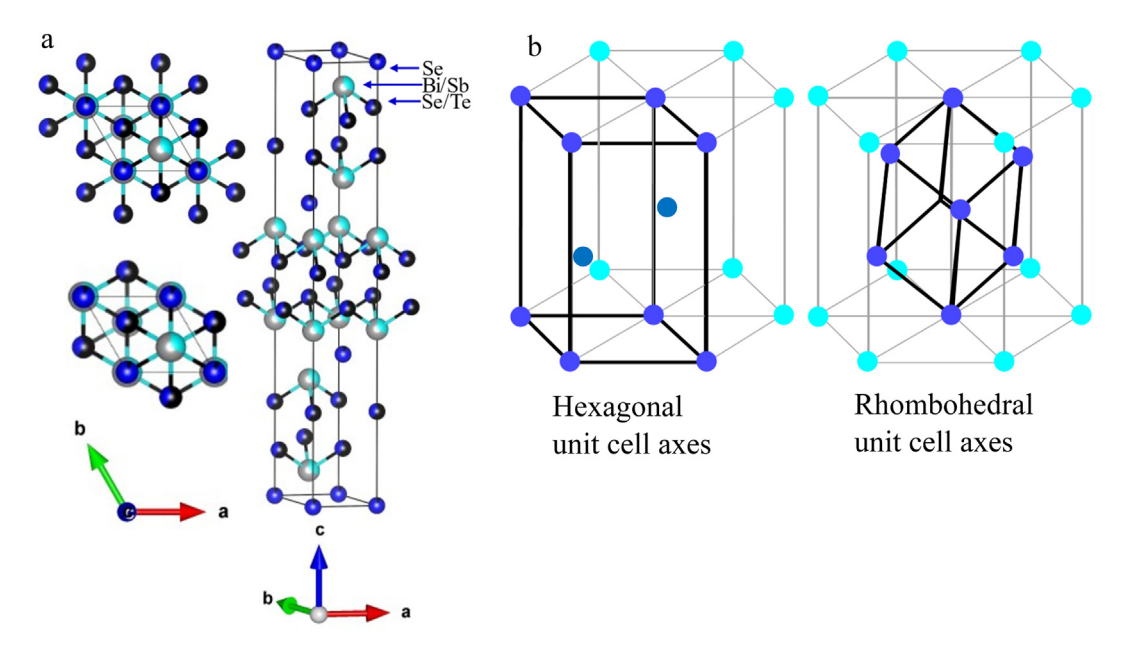


Fig. 1. Crystal structure visualization. (a) Three views of our rhombohedral BSTS crystal structure illustrated using VESTA. (b) Illustration of hexagonal and rhombohedral (obverse) unit cell axes for the  $R\overline{3}m$  m space group. Lattice points within the unit cells are shown in dark blue.

space group  $R\overline{3}m$  (see CSD 2110541in the ICSD database or the full .cif file in supplemental material). Our crystal structure is illustrated in Fig. 1(a).

This agrees with previous work done by Ren et al. [21] and Han et al. [18] which also placed BSTS in the  $R\overline{3}m$  space group. With several structural analyses pointing towards rhombohedral  $R\overline{3}m$  symmetry, we began investigating reports of hexagonal symmetry. Our survey of the literature suggests that at least part of the confusion is rooted in improper use or interpretation of crystallographic terminology. Before we discuss the problems, we first briefly describe some terms related to crystal structure.

A fully defined *crystal structure* includes information about the lattice and the basis. The lattice defines the lengths and angles between identical points ("lattice points") in the repeating structure along with the symmetry elements that relate them. This information is conveyed through unit cell dimensions and space group symmetry. The basis defines the atoms, atomic positions, occupancies, and atomic displacement parameters upon which the symmetry elements operate. Together, the basis, unit cell dimensions, and space group symmetry define a specific crystal structure.

Crystal structure *types* are also commonly used to describe atomic structure. A crystal structure type encompasses materials having the

same space group symmetry but different compositions. For example, NaCl and AgF both belong to the rock salt crystal structure type with  $Fm\overline{3}m$  symmetry and atoms at (0,0,0) and  $(\frac{1}{2},\frac{1}{2},\frac{1}{2})$ .

Crystal systems are large groups of space groups whose point groups have one or more point symmetry elements in common. There are seven crystal systems in crystallography into which the 32 point groups and 230 space groups can be partitioned (see Table 1) [29]. The crystal systems have characteristic unit cell settings (also described in Table 1) that are a result of the required point symmetry and the need to form unit cells that stack without overlaps or gaps. Based on these characteristic unit cell shapes, crystals can also be partitioned into seven different lattice systems or six different crystal families.

Several possible sources of confusion between hexagonal and rhombohedral symmetry are readily apparent from Table 1. First, note that there is not a rhombohedral crystal system; the rhombohedral lattice system is a subset of the trigonal crystal system. The trigonal and hexagonal crystal systems are differentiated by whether a 3-fold or 6-fold axis of symmetry is present, respectively (see Table 1 and the space group diagrams in Fig. 2). Despite this difference, the unit cells of *all* crystals in both the trigonal and hexagonal systems can have the settings

Table 1

The seven crystal systems in crystallography with the point symmetry elements that define them [29]. The number of point groups and corresponding space groups within each crystal system are provided, along with the unit cell settings possible for each crystal system. The characteristic unit cell settings give rise to the lattice system of classification as well as the crystal families indicated.

Crystal System	Point symmetry element(s)	Point Groups	Space Groups	Unit Cell Settings	Lattice System	Crystal Family
Cubic	four 3-fold axes of rotation	5	36	$a=b=c, \alpha=\beta=\gamma=90^\circ$	Cubic	Cubic
Hexagonal	one 6-fold axis of rotation	7	27	$a=b  eq c$ , $lpha=eta=90^\circ$ , $\gamma=120^\circ$	Hexagonal	Hexagonal
Trigonal	one 3-fold axis of rotation	5	18	$a=b  eq c$ , $lpha=eta=90^\circ$ , $\gamma=120^\circ$	Hexagonal	Hexagonal
			7	$a=b\neq c,$ $\alpha=\beta=90^{\circ},$ $\gamma=120^{\circ}$ "hexagonal axes" or $a=b=c,$ $\alpha=\beta=\gamma\neq90^{\circ}$ "rhombohedral axes"	Rhombohedral	Hexagonal
Tetragonal	one 4-fold axis of rotation	7	68	$a=b  eq c$ , $\alpha=\beta=\gamma=90^\circ$	Tetragonal	Tetragonal
Orthorhombic	three perpendicular 2-fold axes of rotation or inversion	3	59	$a  eq b  eq c,  lpha = eta = \gamma = 90^\circ$	Orthorhombic	Orthorhombic
Monoclinic	one 2-fold axis of rotation or one mirror plane	3	13	$a  eq b  eq c$ , $\alpha = \gamma = 90^\circ$ , $\beta =  ext{free}$	Monoclinic	Monoclinic
Triclinic	none	2	2	$a \neq b \neq c, \alpha \neq \beta \neq \gamma$	Triclinic	Triclinic
		32 total	230 total			

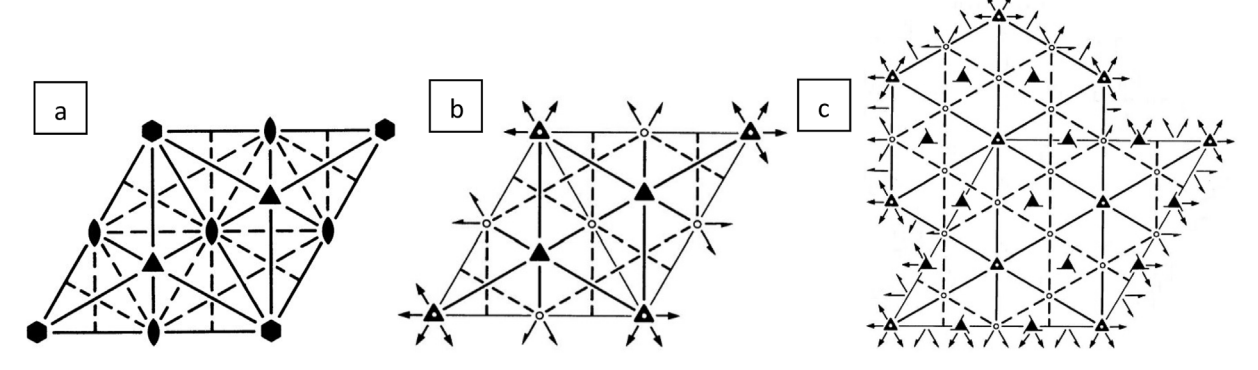


Fig. 2. Space group diagrams for a) the hexagonal space group P6mm, b) the trigonal space group  $P\overline{3}m1$ , and c) the trigonal space group  $R\overline{3}m$ .

 $a=b \neq c$ ,  $\alpha=\beta=90^\circ$ , and  $\gamma=120^\circ$ . These are referred to as "hexagonal axes" [24] because when packed into a crystal, they produce a hexagonally shaped repeating pattern (see Fig. 1(b)). For this reason, both the trigonal and hexagonal crystal systems are sometimes collectively referred to as the hexagonal *crystal family*.

Incorrectly interchanging the terms crystal structure with either crystal system and/or crystal family is a major source of confusion. A prime example is the statement by Ko et al. saying "... the crystal structure of BSTS: a hexagonal crystal structure with a rhombohedral unit cell ..." [19] It is probable the authors meant that BSTS is in the hexagonal crystal family, but the term actually employed was hexagonal crystal structure. This is problematic because the phrase "hexagonal crystal structure" implies that BSTS must have hexagonal space group symmetry, which cannot be true if BSTS has a rhombohedral unit cell and is therefore in the trigonal crystal system. An alternate interpretation is that the authors were using the phrase "hexagonal crystal structure" as a crystal structure type. However, this is also problematic because there is no structure type named hexagonal; with 27 different space groups in the hexagonal crystal system, "hexagonal" is too broad to define a structure type. This is an example of how improper use of crystallographic terminology conveys incorrect meaning.

A further complication is that the trigonal crystal system can be subdivided into two groups. For the first group consisting of 18 space groups, the unit cell setting of  $a=b\neq c$ ,  $\alpha=\beta=90^\circ$ , and  $\gamma=120^\circ$  is the only valid unit cell (for example see Fig. 2(b)). That is why these 18 space groups are classified as part of the hexagonal lattice system. However, for the second group consisting of 7 space groups, the unit cell can be defined either with hexagonal axes  $a=b\neq c$ ,  $\alpha=\beta=90^\circ$ , and  $\gamma=120^\circ$  or with "rhombohedral axes" a=b=c,  $\alpha=\beta=\gamma\neq90^\circ$  (see Fig. 2(c)), which are so termed because they define a traditional rhombohedron [24]. These 7 space groups are given their own lattice system: rhombohedral. Thus, the trigonal crystal system contains 25 space groups all with a 3-fold axis of symmetry, but 18 of these space groups are classified under the hexagonal lattice system and 7 space groups are classified under the rhombohedral lattice system.

The reason for subdividing the trigonal crystal system into two

different lattice systems is the presence of two additional lattice points. The 18 trigonal space groups in the hexagonal lattice system have lattice points only at (0,0,0), or in other words, only at the corners of the unit cell. This makes them "primitive" unit cells, which is why all 18 of these space groups begin with the letter "P" (see Table 2). Set in their hexagonal axes, the 7 remaining trigonal space groups have two additional lattice points *inside* the unit cell either at the obverse setting of (2/3, 1/3, 1/3) and (1/3, 2/3, 2/3) or at the reverse setting of (2/3, 1/3, 2/3) and (1/3, 2/3, 1/3). They are thus "centered" lattices, or unit cells with lattice points in locations other than the corners. The rhombohedral unit cell is produced by using the origin (0, 0, 0) and the two interior lattice points as the corners of the (now primitive) unit cell (see Fig. 1(b)). Because the unit cell of these 7 trigonal space groups can either be a primitive rhombohedron or have "rhombohedrally centered" hexagonal axes, their space group symbols all begin with the letter "R" (see Table 2).

The ability of the 7 rhombohedral space groups to interchange between unit cells with primitive rhombohedral axes and rhombohedrally centered hexagonal axes is the origin of the statement by Lohani et al. that "... shows the primitive unit cell of BiSbTeSe<sub>2</sub> which has a rhombohedral symmetry. This structure can also be depicted as a hexagonal unit cell as shown ..." [20] This statement is perfectly clear and correct, given the in-depth knowledge of crystal systems and lattice systems just outlined. However, this level of familiarity with crystallographic terminology is uncommon due to the cursory (or complete lack of) crystallographic training in higher education today. Thus, when phrases such as "hexagonal unit cell" are used, many investigators innocently but incorrectly assume hexagonal space group symmetry is implied. Misinterpretation of crystallographic terminology is thus also a large problem, either when the terms are used essentially correctly as in Lohani et al. [20] or incorrectly as in Ko et al. [19].

Another prime example of how crystallographic terminology can be easily misinterpreted comes from the scientific software CALPHAD (Computer Coupling of Phase Diagrams and Thermochemistry) provided by the ThermoCalc. As discussed in the introduction, the phase diagram generated for the BSTS stoichiometry suggests the possibility of two different phases, "hexagonal\_A8" and "rhombohedral\_A7" [23]. The A8

**Table 2**Trigonal vs hexagonal crystal systems with space groups listed.

Crystal System	Point symmetry element(s)	Point Groups	Spac	ce Groups	Lattice System	Crystal Family
Hexagonal	one 6-fold axis	7	27	P6, P6 <sub>1</sub> , P6 <sub>5</sub> , P6 <sub>2</sub> , P6 <sub>4</sub> , P6 <sub>3</sub> , P <del>6</del> , P6/m, P6 <sub>3</sub> /m, P622, P6 <sub>1</sub> 22, P6 <sub>5</sub> 22, P6 <sub>2</sub> 22, P6 <sub>4</sub> 22, P6 <sub>3</sub> 22, P6mm, P6cc, P6 <sub>3</sub> cm, P <del>6</del> mc, P <del>6</del> m2, P <del>6</del> c2, P <del>6</del> 2 m, P <del>6</del> 2c, P6/mmm, P6/mcc, P6 <sub>3</sub> /mcm, P6 <sub>3</sub> /mmc	Hexagonal	Hexagonal
Trigonal	one 3-fold axis	5	18	P3, P3 <sub>1</sub> , P3 <sub>2</sub> , P $\overline{3}$ , P312, P321, P3 <sub>1</sub> 12, P3 <sub>1</sub> 21, P3 <sub>2</sub> 12, P3 <sub>2</sub> 21, P3m1, P31 m, P3c1, P31c, P $\overline{3}$ 1m, P $\overline{3}$ 1c, P $\overline{3}$ m1, P $\overline{3}$ c1	Hexagonal	Hexagonal
			7	R3, R3, R32, R3m, R3c, R3m, R3c	Rhombohedral	Hexagonal

and A7 labels are Strukturbericht designations originally developed by Zeitschrift für Kristallographie [24] and which have passed out of usage. Thus, users of the software rely primarily on the first part of the label (hexagonal or rhombohedral) to differentiate the two options and may erroneously assume either hexagonal or rhombohedral space group symmetry is implied. Only those determined users who do the work to tie these labels to modern IUCr nomenclature find that both structures are in the trigonal crystal system; the A7 Strukturbericht designation corresponds to space group 166 with  $R\overline{3}m$  symmetry and A8 Strukturbericht corresponds to space group 152 with  $P3_121$  symmetry. It is problematic that CALPHAD labels these phases with outdated nomenclature because users could unintentionally misinterpret what must be a lattice system label as an indication of space group symmetry.

One final source of misinterpretation is the convention to use hexagonal axes for the rhombohedral space groups. Due to the ease of calculation afforded by right angles, modern software almost exclusively uses hexagonal axes for all trigonal space groups (for example, see our current rhombohedral structure). Perhaps because of the "hexagonal" label and certainly because of cursory crystallographic training, hexagonal axes  $a=b\neq c$ ,  $\alpha=\beta=90^\circ$ , and  $\gamma=120^\circ$  are only associated with hexagonal symmetry for a majority of the scientific population. Thus, when indexing algorithms for X-ray or electron diffraction data provide a unit cell with hexagonal axes, a vast majority of users may assume hexagonal (or 6-fold) symmetry is implied, when in reality either 6-fold (hexagonal) or 3-fold (trigonal) symmetry is possible.

To summarize, miscommunication is a significant source of confusion for the symmetry of BSTS. Either improper use of crystallographic terminology or misinterpretation of it has led to crystal symmetry being confused with lattice system, crystal family, and unit cell axes. As Table 1 shows, the overlap between these various classification systems can be easily confusing; however, the root of the problem lies in inadequate crystallographic training. This exemplifies why training in fundamental concepts and terminology of solid state science is still essential for modern materials scientists.

#### 3.2. Powder XRD

Recall that CALPHAD predicts the  $P3_121$  phase to be 3 times more stable than the  $R\overline{3}m$  phase with Gibbs free energies of formation of  $G_{P3_121,f,300C}=-600~kJ/mol$  and  $G_{R\overline{3}m,f,300C}=-150~kJ/mol$ , respectively. This runs contrary to our own experimental observations as well as those by Ren et al. [21] and Han et al. [18] which show  $R\overline{3}m$  symmetry as the primary symmetry for BSTS. However, one crystal may not be representative of the entire batch; it is possible that a mixture of phases was present.

To determine how representative the  $R\overline{3}m$  single crystal was of our entire batch of BSTS, powder XRD data were collected and compared to representative trigonal  $P\overline{3}m1$  and rhombohedral  $R\overline{3}m$  phases through phase matching and Rietveld refinement (Fig. 3). (The trigonal space group  $P\overline{3}m1$  was selected instead of  $P3_121$  because no compound was found in the database with BSTS stoichiometry in space group  $P3_121$ . In addition, no hexagonal BSTS structures could be tested via Rietveld refinement because none of the reported hexagonal structures contain atom positions.) As Fig. 3 shows, the  $R\overline{3}m$  structures adequately explain the positions of all peaks in the powder XRD data whereas the  $P\overline{3}m1$  structure does not.

## 3.3. Atom occupancies

An interesting aspect of the BSTS material is its variable stoichiometery:  $Bi_{2-x}Sb_xTe_{3-y}Se_y$ . In our sample, the raw materials were mixed with a ratio of 1:1:1:2 Bi: Sb: Te: Se, but the ratios actually achieved in the final BSTS material must be experimentally determined. In our single crystal XRD analysis, it was assumed that Bi and Sb substitute for one another in the lattice and that Te and Se substitute for one

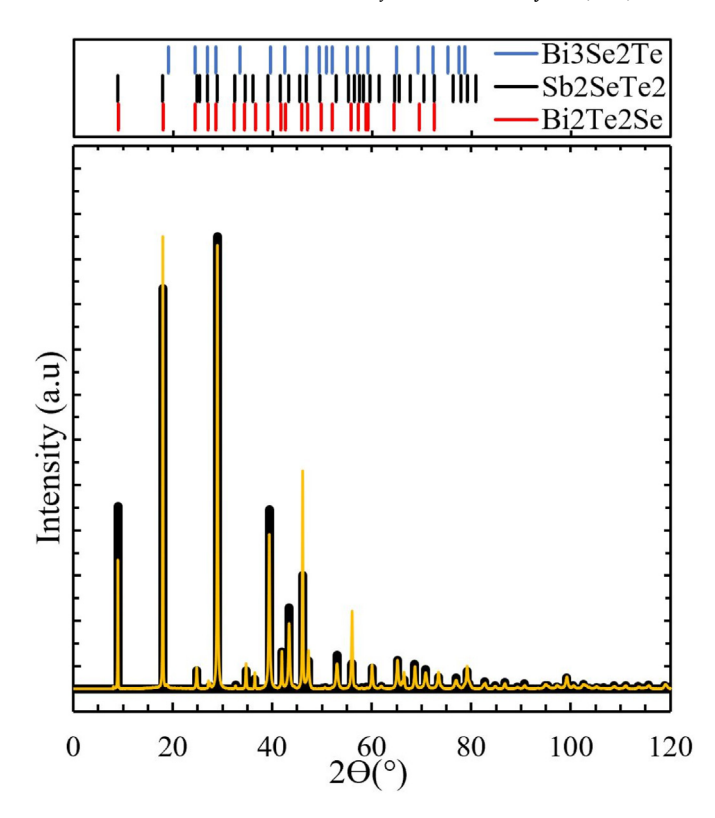


Fig. 3. Our BSTS powder XRD pattern (orange) with the Rietveld refinement (black) compared to the trigonal telluronevskite ( $Bi_3Se_2Te$ ) space group  $P\overline{3}m1$ , trigonal antimony selenium telluride ( $Sb_2SeTe_2$ ) space group  $R\overline{3}m$ , and trigonal Kawazuite ( $Bi_2Te_2Se$ ) space group  $R\overline{3}m$ .

another in the lattice. These assumptions were based on chemical considerations and are in agreement with Han et al.'s previous analysis (CSD 1864200). The asymmetric unit contained three unique atom sites. Each site was modeled as a mixture of two atoms: either a Te/Se mixture or a Bi/Sb mixture. Two of the unique positions in the asymmetric unit corresponded to Te/Se mixtures, and one corresponded to Bi/Sb. Each pair of atoms were constrained to have equal coordinates (EXYZ) and equal anisotropic displacement parameters (EADP). The occupancies of the atoms in each pair were allowed to refine with the constraint that together they add to constitute a fully occupied site. Three different starting ratios of the occupancies were used in different refinements to test the reliability of the occupancies: (1) the ratios reported in Han et al.'s study which were Bi = 0.56/Sb = 0.44, Te = 0.65/Se = 0.35, Te = 0.440.06/Se = 0.94; (2) ratios in which the minor component of each site was set to zero, namely Bi = 1/Sb = 0, Te = 1/Se = 0, Te = 0/Se = 1; and (3) equal occupancies (0.5) for all atom types. The opposite of option (2) was also attempted but was unstable. Despite the different starting points, the occupancies of all refinements converged to the ratios reported in the current structure: Bi = 0.620 (3)/Sb = 0.380 (3); Te = 0.590 (3)/Se = 0.5900.410 (3); Te = 0.082 (3)/Se = 0.918 (3). These ratios are thus unambiguously the best description of the occupancies for the single crystal used in this experiment, leading to a chemical formula of Bi<sub>1.24</sub>Sb<sub>0.76</sub>- $Te_{1.26}Se_{1.74}$  and a density of 7.38 g/cm<sup>3</sup>.

As Table 3 shows, the unit cell parameters and atom positions remained similar in both the single crystal and powder refinements. However, the peak height ratios predicted by the single crystal structure were significantly different than the peak height ratios observed in the powder data, leading us to refine the occupancy ratios of the atom pairs in the three unique sites (Bi/Sb, Te1/Se1, Te2/Se2). This still did not adequately model the peak height ratios, and upon inspection, preferred orientation in the (003) family was apparent in the data, with several peaks being severely under-fit by the initial structure: (003) at  $\sim$ 9° 20, (006) at  $\sim$ 18° 20, (0015) at 46° 20, and (0018) at  $\sim$ 56° 20. Modeling this

**Table 3**Comparison of crystal structure parameters derived from Han et al. (CSD 1864200), our single-crystal (SC-XRD) analysis (CSD 2110541), and our powder (P-XRD) Rietveld refinement. In addition to the lattice parameters and densities, the variable z coordinates for the two 6c sites and the site occupancy factor (s.o.f) ratios for all three unique atom sites are shown.

	Han (1864200)	SC-XRD (2110541)	P-XRD
Temperature	273 K	100 K	295 K
a(Å)	4.187 (2)	4.1512 (9)	4.168
b(Å)	4.187 (2)	4.1512 (9)	4.168
c(Å)	29.648 (16)	29.390 (9)	29.515
α	90°	90°	90°
β	90°	90°	90°
γ	120°	120°	120°
Site 1: 6c (z)	0.39654 (4)	0.39692 (2)	0.3980
Site 2: 6c (z)	0.21296 (7)	0.21260(3)	0.2109
Site 1 Bi/Sb s.o.f	0.56(6)/0.44(6)	0.620(3)/0.380(3)	0.62/0.38
Site 2 Te/Se s.o.f	0.65(8)/0.35(8)	0.590(3)/0.410(3)	0.59/0.41
Site 3 Te/Se s.o.f	0.06(8)/0.94(8)	0.082(3)/0.918(3)	0.08/0.92
Density (g/cm <sup>3</sup> )	6.822	7.381	7.29
Space Group	$R\overline{3}m$	R <del>3</del> m	$R\overline{3}m$

preferred orientation using spherical harmonics significantly improved the fit, particularly for the (003) and (006) peaks. However, the occupancy parameters were highly correlated with the parameters correcting for the preferred orientation, so the occupancies were fixed to those determined in the single crystal analysis. Several other models were attempted to see if the predicted peak height ratios could be improved. Metallic Bi and Sb phases were added to the BSTS phase in mixed-phase refinements, but the phase fraction of these additional phases refined to zero each time. Similarly, two rhombohedral BSTS phases with differing element ratios were attempted in a mixed-phase refinement, but the fit was not improved over the single-phase refinement, and the refinement was greatly destabilized. Since the experiment was conducted in air over several hours, one other possibility that could not be effectively modeled is oxygen or water contamination of the sample.

The single-phase structural model in the  $R\overline{3}m$  space group shown in Fig. 3 thus proved the best model for the powder XRD data. The model is not perfect, but the imperfections all lie in the predicted peak height ratios, which we attribute to difficulties modeling preferred orientation simultaneously with site occupancies or possibly to deterioration/contamination of the sample in air. The peak positions are all correctly predicted by the rhombohedral phase, so our single crystal structure with  $R\overline{3}m$  space group symmetry seems reasonably representative of our entire batch of BSTS. We therefore conclude that our synthetic conditions produce essentially phase pure BSTS with  $R\overline{3}m$  symmetry.

Comparing all three detailed XRD analyses of BSTS available, it appears that while the rhombohedral character of BSTS is consistent, there are some small variations in unit cell parameters, atom site occupancy factors, and therefore density from crystal to crystal and batch to batch. As Table 3 highlights, the two single crystal models share similar Bi/Sb ratios, but the densities differ due to a constriction in the unit cell parameters in our single crystals. This constriction could be attributed in part to the low temperature (100 K) of our analysis compared to that of Han et al. (273 K), but our powder analyses at 295 K show that even at temperatures above Han et al.'s, our BSTS sample appears to have smaller unit cell parameters and thus a higher density. Such variations between crystals and/or batches are not unexpected, but they could be an important source of performance variation from batch to batch for the BSTS material.

#### 3.4. TEM

Electron diffraction in TEM is commonly used to index materials, so electron diffraction was conducted as a secondary means of verifying our single crystal structure. The TEM images of our own BSTS (Fig. 4) highlight what we believe is the largest source of the confusion surrounding the BSTS crystal structure: twinning. At the low magnification shown in Fig. 4(a), the spot pattern appears hexagonal. However, upon closer investigation at higher magnification as shown in Fig. 4(b), nearly every reflection is clearly a doublet. Such non-overlapping spots are characteristic of non-merohedral twinning, in which two crystallites with different and unrelated orientations grow in close proximity and eventually fuse into one particle that nevertheless gives two distinct diffraction patterns. Twinning is common in the trigonal crystal system with  $R\overline{3}m$  space group [30], but the twinning in BSTS is particularly pernicious because it verges on merohedral twinning in which the two spot patterns overlap essentially exactly and in a way that mimics a higher symmetry: hexagonal.

The twinning observed in the TEM images was also observed in the XRD analyses; several twinned crystals were screened and rejected before finding a thin fragment ( $\leq 8~\mu m$  thick) that was single crystalline. Once we realized how ubiquitously twinning was observed in BSTS, we sought to identify the twin law (or the mathematical relationship between the unit cells of the different domains). For, if twinning is observed so consistently, then the twin law is probably also consistent. We returned our attention to a small set of preliminary XRD data collected for a crystal that was rejected during the single crystal XRD analysis. Using the 738 reflections harvested from the 60 preliminary images, we identified multiple potential secondary domains using *CELL\_NOW*, each of which

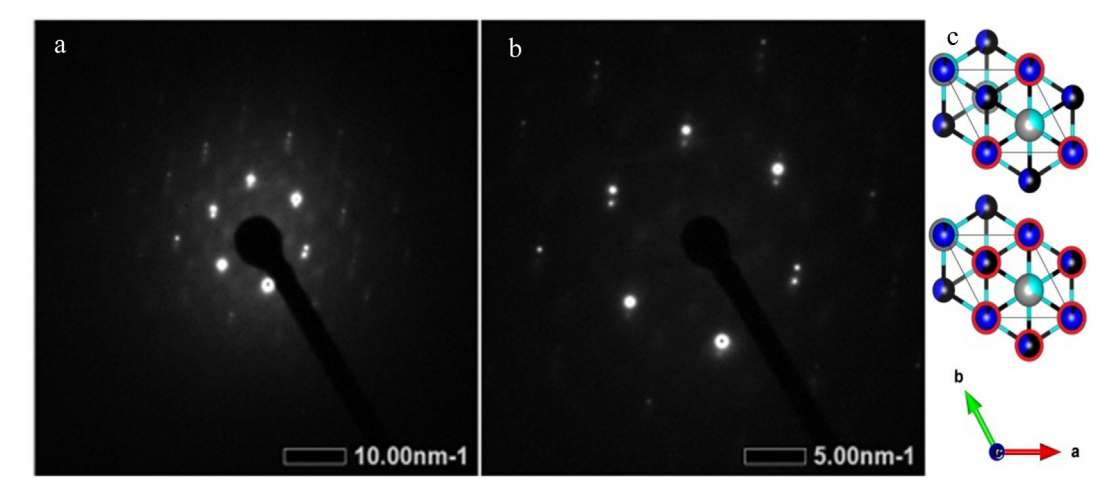


Fig. 4. Electron diffraction images of BSTS at (a) low magnification and (b) high magnification. (c) Renderings of the  $R\overline{3}m$  BSTS structure viewed down the *c*-axis. In the topmost rendering, points related by the 3-fold symmetry are highlighted in red. In the bottom rendering, points highlighted in red are those that would *appear* to be related by a 6-fold axis if two domains with 3-fold axes rotated by  $180^{\circ}$  were present.

was related to the primary domain by *nearly*  $180^{\circ}$  rotation about *approximately* the *c*-axis (or [001] direction): for example, a  $179.8^{\circ}$  rotation about the [0.124, 0.110, 1.0000] real axis or a  $179.9^{\circ}$  rotation about the [-0.008, 0.099, 1.000] real axis.

Recall from the discussion of Table 1 that the primary difference between trigonal and hexagonal crystal systems is whether a 3-fold or 6-fold axis of symmetry lies parallel to the c-axis (of the unit cell with hexagonal axes), as illustrated in Fig. 2. If the 3-fold axes of two fused domains are collinear but one domain is rotated 180° around that axis relative to the other domain, then, as illustrated in Fig. 4(c), the two 3-fold axes will mimic one 6-fold axis. In the case of our BSTS in which each domain has  $\overline{3}m$  symmetry, the two overlapping diffraction patterns would look like one pattern with 6/mmm symmetry, thereby appearing deceptively hexagonal.

The slight imperfection of the 2-fold rotation relating the domains in our BSTS crystal (i.e.,  $179^{\circ}$  instead of exactly  $180^{\circ}$ ) was fortuitous in that the multiple diffraction patterns did not perfectly overlap, enabling us to observe and identify the twinning effect. Others may not have been so fortunate; BSTS crystals with more perfect twinning would be deceptively hexagonal and extremely difficult to parse into the true trigonal components.

There are actually two possible twin laws for BSTS. Because the  $R\overline{3}m$  space group is centrosymmetric (has a center of inversion), a 2-fold rotation about the c-axis is equivalent to a reflection across the ab plane, as the matrices for these twin laws are related by inversion [31]. Thus, the twin law(s) for BSTS crystals could be either

$$\begin{pmatrix} -1 & 0 & 0 \\ 0 & -1 & 0 \\ 0 & 0 & 1 \end{pmatrix}$$
 in the case of 2-fold rotation about the *c*-axis,

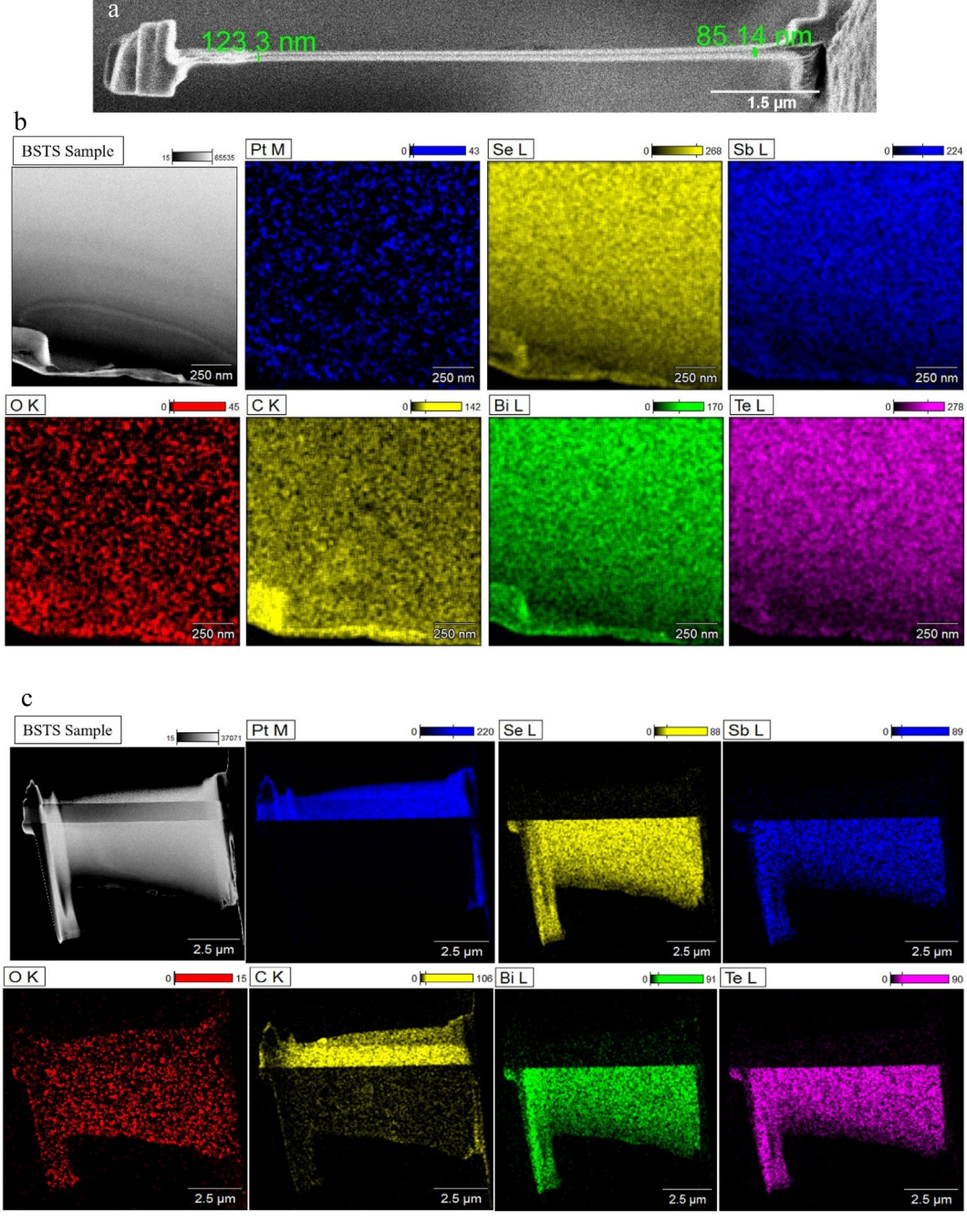


Fig. 5. (a) TEM sample cut by FIB. (b) TEM-EDS elemental mapping. (c) SEM-EDS elemental mapping.

or 
$$\begin{pmatrix} 1 & 0 & 0 \\ 0 & 1 & 0 \\ 0 & 0 & -1 \end{pmatrix}$$
 for a reflection across the  $ab$  plane.

Our analysis has focused on the 2-fold rotation twin law since this was the law determined for our crystal by *CELL\_NOW*. This is not definitive proof, however, since this program searches exclusively for twinning by rotation. In fact, distinguishing these twin laws is not possible from diffraction data alone; the two can only be differentiated by examining the atomic structure itself [31]. Considering the packing that would be produced by each twin law at the interface of the two domains, we did not see a significant advantage for one twin law over the other and conclude that both are possible/plausible.

We therefore propose that the primary source of confusion behind the BSTS crystal structure stems from nearly merohedral twinning by 2-fold rotation about the c-axis and/or by reflection across the ab plane. Such twinning causes the true trigonal  $\overline{3}m$  symmetry of the individual domains to appear (incorrectly) as hexagonal 6/mmm symmetry. While this twinning does not seem to inhibit material performance (indeed, it may enhance or be necessary for performance), it complicates structural analysis. In diffraction experiments, such twinning may go unnoticed during the determination of the lattice parameters; investigators may not become aware of the issue until later when a suitable space group cannot be found or reasonable atom positions cannot be found. This could be why no atom positions have been reported for any hexagonal BSTS structures.

#### 3.5. TEM-EDS

In addition to the electron diffraction data discussed above, TEM-EDS data were collected to ensure that the material had retained its elemental composition. Preparing a BSTS sample thin enough for TEM was challenging because BSTS consists of low-melting-temperature materials. The BSTS crystal prepared by FIB was coated with Pt and then cut by a laser, producing a layer of material with a thickness of about 80 nm, as shown in Fig. 5(a). Fig. 5(b) confirms that Bi, Sb, Te, and Se are present and dispersed throughout the crystal as expected. However, significant amounts of oxygen and carbon were detected as well. Futher investigations using SEM-EDS on the elemental compostion over a larger range of the sample (Fig. 5(c)) confirmed the presence of C and O, though SEM showed more oxygen than carbon.

#### 3.6. XPS

XPS was employed to further investigate the presence of oxygen and carbon on our BSTS TEM sample. Fig. 6 shows the full range of XPS data collected on our BSTS sample before and after sputtering along with the relative quantities of elements present. As the pie charts in 6(b) and 6(c) show, sputtering reduced the oxygen content by  $\sim$ 2/3 and the carbon content by  $\sim$ 1/3. This shows that the oxygen at least is primarily adsorbed at the surface.

To investigate where the oxygen is adsorbing, the bonding environment of each element was scrutinized before and after sputtering. XPS detects electron binding energies of elements at the surface of a sample, so changes in these binding energies indicate changes in the bonding environments of the element. As Fig. 7 shows, the oxygen was primarily associated with Bi and Sb. No oxygen was associated with Se, and the small amount that was associated with Te was completely removed by sputtering. Bi and Sb thus appear to have similar chemical affinity towards oxygen while Te and Se have a similar disinclination towards oxygen. This provides some validation for our assumption in the XRD analyses that Bi and Sb would display similar chemical behavior and so substitute for one another in the lattice while Te and Se would display similar chemical behavior and substitute for one another in the lattice

While Bi and Sb both adsorbed oxygen initially, sputtering had different effects on the oxygen adsorption of these two elements. Sputtering decreased the amount of oxygen associated with Sb by nearly half while it had a minimal (almost negligible) effect on Bi. Bi thus appears to have the greatest affinity for oxygen in BSTS, so surface Bi sites are the most likely sources of oxygen contamination in BSTS.

The element quantifications afforded by the XPS anlayses also provide some confirmation for the Bi/Sb and Te/Se ratios determined in the single crystal XRD analysis. From Fig. 7(b) and (c), the Bi/Sb ratios before and after sputtering were 0.63/0.37 and 0.61/0.39, respectively, which are precisely in line with the 0.62/0.38 ratio determined in the SC-XRD analyses. The Te/Se ratios from the XPS analyses (0.33/0.67 before and 0.30/0.70 after sputtering) varied more from the ratios determined in the XRD analyses (0.42/0.58), though all agree that Te is present in smaller quantities than Se, as we anticipated from the synthetic conditions.

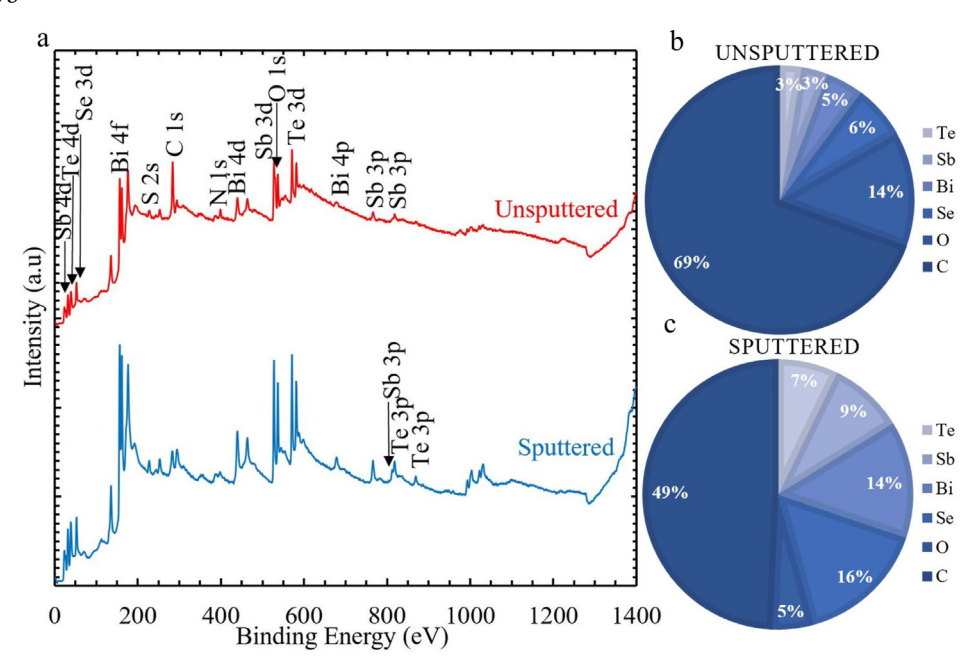


Fig. 6. (a) Full range of XPS data for BSTS before and after sputtering with the relative quantities of each element before (b) and after (c) sputtering.

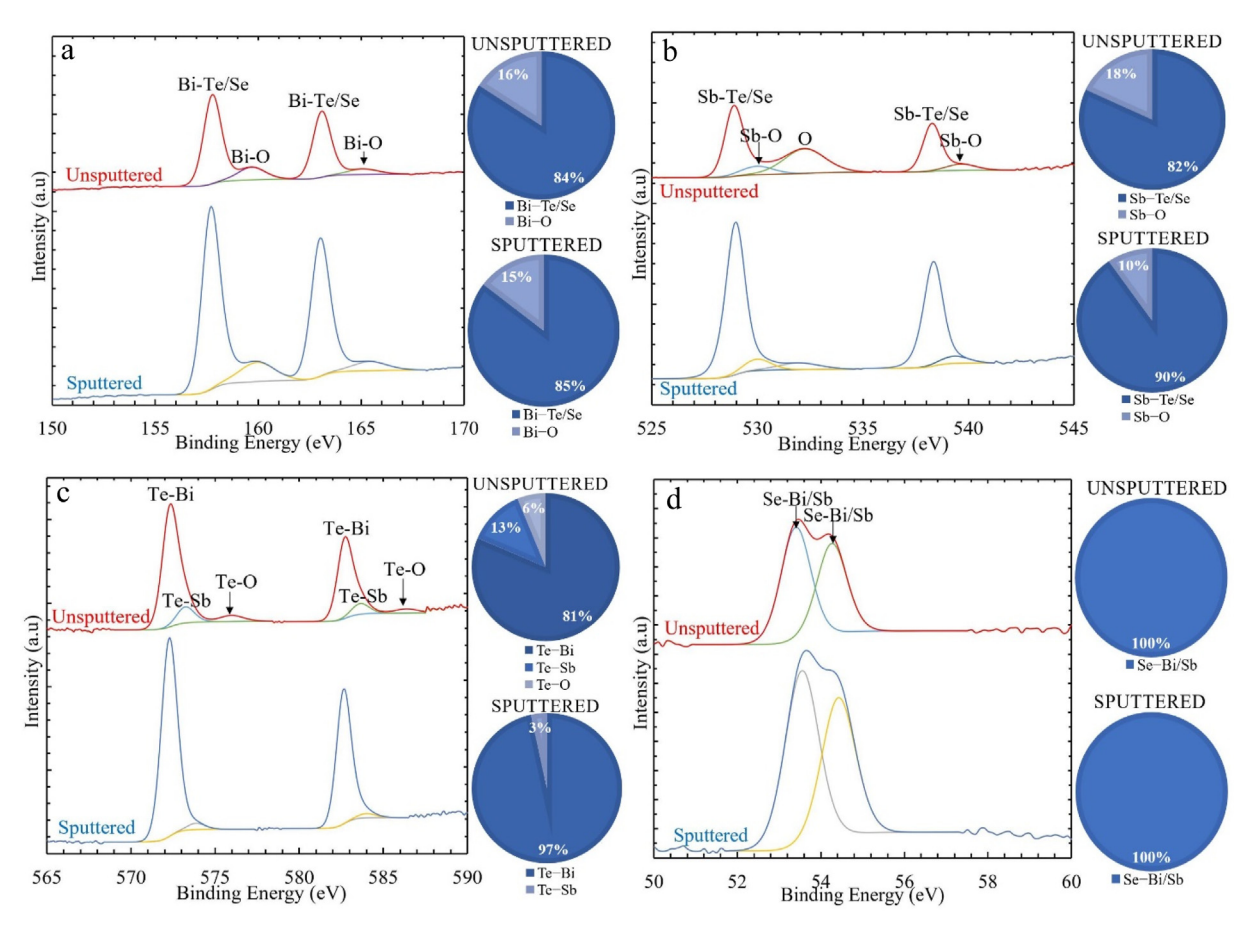


Fig. 7. XPS data before and after sputtering for the (a) Bi 4f, (b) Sb 3d, (c) Te 3d, and (d) Se 3d regions. Overlaid with the data are the fits used to deduce the relative quantities of bonding environments that are shown in the accompanying pie charts.

#### 3.7. XRF

The XPS data left some ambiguity as to whether all or only some of the O and C content was adsorbed at the surface. While a majority ( $\sim$ 2/3) of the oxygen content could be attributed to surface adsorption at primarily Bi and Sb sites,  $\sim$ 1/3 of the oxygen content and  $\sim$ 2/3 of the carbon content was not removed by sputtering. To investigate the possibility that these elements had been incorporated into the lattice during crystal growth, we used XRF to quantify the elements present in a BSTS bulk sample. We gently cleaved a cross-section from the middle of a solid BSTS sample as illustrated in Fig. 8, then examined the elemental composition over a large area. As Fig. 8 shows, the XRF bulk scan did not detect any O or C. This confirms that all of the O and C detected via TEM-EDS, SEM-EDS, and XPS analyses was due to surface adsorption during FIB processing. As with the XPS data, the XRF element ratios (Bi/Sb = 0.62/0.38, Te/Se = 0.27/0.73) confirm the Bi/Sb ratios determined via XRD (0.62/0.38).

#### 4. Conclusions

BSTS crystals have been investigated using multiple techniques to determine the BSTS crystal structure and understand the origin of conflicting reports of both hexagonal and rhombohedral symmetry. Single crystal XRD analysis of our own BSTS produced an excellent structure ( $R_1=1.8\%,\ wR_2=4.3\%$ ) in the trigonal crystal system with a rhombohedral lattice defined by space group  $R\overline{3}m$  (CSD 2110541). However, we encountered pernicious non-merohedral twinning in both our XRD and electron diffraction experiments that verged on merohedral twinning, mimicking a hexagonal lattice. We therefore propose that the

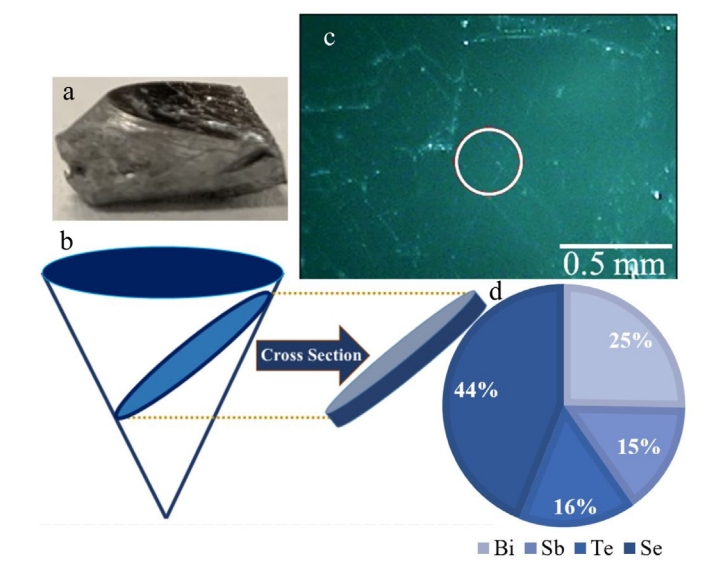


Fig. 8. XRF BSTS analysis. (a) BSTS grown crystal sample, (b) sample cross-section diagram, (c) XRF scan image, and (d) elemental distribution pie chart.

primary source of confusion for the symmetry of BSTS stems from ubiquitous twinning in which the twin law (either a 2-fold rotation about the c-axis and/or a reflection across the ab plane) causes the true trigonal  $\overline{3}m$  symmetry of the individual domains to appear (incorrectly) as

hexagonal 6/mmm symmetry. A secondary source of confusion is the improper use or misinterpretation of crystallographic terminology, which has led to crystal symmetry being incorrectly confused with lattice system, crystal family, or unit cell choice.

Powder XRD analyses confirmed that our BSTS was phase pure and best described as rhombohedral. Comparing all three rhombohedral XRD analyses available, there are small variations in unit cell parameters, atom site occupancy factors, and therefore density from crystal to crystal and batch to batch. Such variations are not unexpected, but they could be an important source of performance variation from batch to batch for the BSTS material.

TEM-EDS, XPS, and XRF analyses revealed that even though our BSTS is phase pure, the surface has a tendency to adsorb oxygen and carbon. XPS analysis showed that the oxygen is primarily adsorbed by Bi and Sb. Sputtering can decrease the oxygen adsorbed by Sb, but Bi retains nearly all of its adsorbed oxygen even after sputtering. Surface Bi sites are thus the most likely sources of oxygen contamination in BSTS.

#### Accession codes

CSD 2110541 contains the supplementary crystallographic data for this paper.

#### Work contributions

H.F.A. manuscript preparation, methodology developement, sample synthesis and measurement (TEM, XPS, and XRF), analysis, and manuscript revision. S.J.S performed the single-crystal and powder XRD measurements/analyses, twinning analyses, and manuscript revision. T.D.S. contributed research initiation, supervision, analysis, and manuscript revision.

## CRediT authorship contribution statement

**Husain F. Alnaser:** Methodology, Software, Validation, Investigation, Writing – original draft, Visualization. **Stacey J. Smith:** Software, Validation, Formal analysis, Writing – original draft. **Taylor D. Sparks:** Conceptualization, Resources, Data curation, Writing – review & editing, Supervision, Project administration, Funding acquisition.

#### Declaration of competing interest

The authors declare that they have no known competing financial interests or personal relationships that could have appeared to influence the work reported in this paper.

### Data availability

All raw and processed data are included in the supplemental information.

#### Acknowledgments

This work was primarily supported by NSF QII-TAQS grant # 1936383. T.D.S. acknowledges partial support from the Royal Society Wolfson Visiting Fellowship.

H.F.A. acknowledges partial support by the Kuwait Foundation for the Advancement of Sciences (KFAS) under project code "CB20-68EO-01".

#### Appendix A. Supplementary data

Supplementary data to this article can be found online at https://do i.org/10.1016/j.jssc.2023.123868.

#### References

- Enwei Sun, Wenwu Cao, Relaxor-based ferroelectric single crystals: growth, domain engineering, characterization and applications, Prog. Mater. Sci. 65 (2014) 124–210, https://doi.org/10.1016/j.pmatsci.2014.03.006. Crossref.
- [2] Taro Toyoda, et al., The electronic structure and photoinduced electron transfer rate of CdSe quantum dots on single crystal rutile TiO2: dependence on the crystal orientation of the substrate, J. Phys. Chem. C 120 (4) (2016) 2047–2057, https:// doi.org/10.1021/acs.jpcc.5b09528. Crossref.
- [3] Tatsuyuki Makita, et al., High-performance, semiconducting membrane composed of ultrathin, single-crystal organic semiconductors, Proc. Natl. Acad. Sci. U. S. A 117 (1) (2019) 80–85, https://doi.org/10.1073/pnas.1909932116. Crossref.
- [4] Hui Jiang, Wenping Hu, The emergence of organic single-crystal electronics, Angew. Chem. Int. Ed. 59 (4) (2019) 1408–1428, https://doi.org/10.1002/anie.201814439. Crossref.
- [5] H. Boschker, J. Mannhart, Quantum-matter heterostructures, Annu. Rev. Condens. Matter Phys 8 (1) (2017) 145–164, https://doi.org/10.1146/annurev-conmatphys-031016-025404. Crossref.
- [6] Norman Einspruch, William Frensley, Chapter-1 heterostructure and quantum well physics, in: first ed.Heterostructures and Quantum Devices (ISSN Book 24), Academic Press. 2014, pp. 1–24.
- [7] B. Keimer, J.E. Moore, The physics of quantum materials, Nat. Phys. 13 (11) (2017), https://doi.org/10.1038/nphys4302, 1045–55. Crossref.
- [8] Xiaolong Liu, Mark C. Hersam, 2D materials for quantum information science, Nat. Rev. Mater. 4 (10) (2019) 669–684, https://doi.org/10.1038/s41578-019-0136-x. Crossref.
- [9] Yang Xu, et al., Observation of topological surface state quantum Hall effect in an intrinsic three-dimensional topological insulator, Nat. Phys. 10 (12) (2014) 956–963, https://doi.org/10.1038/nphys3140. Crossref.
- [10] Su Kong Chong, et al., Tunable coupling between surface states of a three-dimensional topological insulator in the quantum Hall regime, Phys. Rev. Lett. 123 (3) (2019), https://doi.org/10.1103/physrevlett.123.036804. Crossref.
- [11] Su Kong Chong, et al., Topological insulator-based van Der waals heterostructures for effective control of massless and massive Dirac fermions, Nano Lett. 18 (12) (2018), https://doi.org/10.1021/acs.nanolett.8b04291, 8047–53. Crossref.
- [12] Su Kong Chong, et al., Landau levels of topologically-protected surface states probed by dual-gated quantum capacitance, ACS Nano 14 (1) (2019) 1158–1165, https://doi.org/10.1021/acsnano.9b09192. Crossref.
- [13] M. Zahid Hasan, Joel E. Moore, Three-dimensional topological insulators, Annu. Rev. Condens. Matter Phys 2 (1) (2011) 55–78, https://doi.org/10.1146/annurev-conmatphys-062910-140432. Crossref.
- [14] Sebastian Bauer, Christian A. Bobisch, Nanoscale electron transport at the surface of a topological insulator, Nat. Commun. 7 (1) (2016), https://doi.org/10.1038/ ncomms11381. Springer Science and Business Media LLC, Apr.
- [15] Y. Pan, et al., Low carrier concentration crystals of the topological insulator Bi2-xSbxTe3-YSey: a magnetotransport study, New J. Phys. 16 (12) (2014), 123035, https://doi.org/10.1088/1367-2630/16/12/123035.
- [16] S.K. Kushwaha, et al., Sn-doped Bi1.1Sb0.9Te2S bulk crystal topological insulator with excellent properties, 1, Nat. Commun. 7 (2016), https://doi.org/10.1038/ ncomms11456. Crossref.
- [17] James G. Analytis, et al., Two-dimensional surface state in the quantum limit of a topological insulator, Nat. Phys. 6 (12) (2010) 960–964, https://doi.org/10.1038/ nphys1861. Crossref.
- [18] Kyu-Bum Han, et al., Enhancement in surface mobility and quantum transport of Bi2-x5bxTe3-ySey topological insulator by controlling the crystal growth conditions, Sci. Rep. 8 (1) (2018), https://doi.org/10.1038/s41598-018-35674-z. Crossref.
- [19] Wonhee Ko, et al., Atomic and electronic structure of an alloyed topological insulator, Bi1.5Sb0.5Te1.7Se1.3, Sci. Rep. 3 (1) (2013), https://doi.org/10.1038/ srep02656. Crossref.
- [20] H. Lohani, et al., Band structure of topological insulator BiSbTe1.25Se1.75, Sci. Rep. 7 (1) (2017), https://doi.org/10.1038/s41598-017-04985-y. Crossref.
- [21] Zhi Ren, et al., Optimizing Bi2-xSbxTe3-ySey solid solutions to approach the intrinsic topological insulator regime, Phys. Rev. B 84 (16) (2011), https://doi.org/ 10.1103/physrevb.84.165311. Crossref.
- [22] Husain Alnaser, Taylor D. Sparks, BSTS Synthesis Guided by CALPHAD Approach for Phase Equilibria and Process Optimization, SSRN Elec. J., 2021, https://doi.org/ 10.2139/ssrn.3920963. Crossref.
- [23] W.L. Bragg, Strukturbericht, 1913–1928, Nature 128 (3230) (1931) 511–512, https://doi.org/10.1038/128511a0. SSBM LLC, Sept.
- [24] Aroyo, I. Mois, International tables for crystallography, space-group symmetry: space-group symmetry, in: Volume A, 6thIUCr Series. International Tables for Crystallography), Wiley, 2017.
- [25] L. Krause, R. Herbst-Irmer, G.M. Sheldrick, D. Stalke, J. Appl. Crystallogr. 48 (2015)
- [26] George M. Sheldrick, Acta Crystallogr. A71 (2015) 3-8.
- [27] George M. Sheldrick, Acta Crystallogr. C71 (2015) 3-8.
- [28] Peter Müller, Crystallography 15 (2009) 57–83.
- [29] Carmelo Giacovazzo, Symmetry in crystals, in: Fundamentals of Crystallography, third ed., Oxford University Press, 2011, pp. 1–65.
- [30] Madhumati Sevvana, et al., Non-merohedral twinning: from minerals to proteins, Acta Crystallogr. D: Struct. Biol. 75 (12) (2019), https://doi.org/10.1107/ s2059798319010179, 1040–50. Crossref.
- [31] Gregory S. Girolami, Examples of twinned crystals, in: X-Ray Crystallography, University Science Books, 2016, pp. 417–426.